metals

MDPI

Article

Effect of the Temperature in the Mechanical Properties of Austenite, Ferrite and Sigma Phases of Duplex Stainless Steels Using Hardness, Microhardness and Nanoindentation Techniques

Gorka Argandoña [1], José F. Palacio [2], Carlos Berlanga [3,4], María V. Biezma [5], Pedro J. Rivero [3,4,*], Julio Peña [1] and Rafael Rodriguez [3,4]

1 Multidisciplinary Centre of Technologies for Industry (CEMITEC), Polígono Mocholí, Noain, 31110 Pamplona, Spain; gargandona@cemitec.com (G.A.); jpena@cemitec.com (J.P.)
2 Centre of Advanced Surface Engineering, AIN, Cordovilla, 31191 Pamplona, Spain; jfpalacio@ain.es
3 Materials Engineering Laboratory, Department of Mechanical, Energetic and Materials Engineering, Public University of Navarre, Campus Arrosadía S/N, 31006 Pamplona, Spain; carlos.berlanga@unavarra.es (C.B.); rafael.rodriguez@unavarra.es (R.R.)
4 Institute for Advanced Materials (INAMAT), Public University of Navarre, Campus Arrosadía S/N, 31006 Pamplona, Spain
5 Department of Earth, Materials Science and Engineering, University of Cantabria, 39004 Santander, Spain; maria.biezma@unican.es
* Correspondence: pedrojose.rivero@unavarra.es; Tel.: +34-948-16-89-61

Received: 29 April 2017; Accepted: 10 June 2017; Published: 14 June 2017

Abstract: The aim of this work is to study the hardness of the ferrite, austenite and sigma phases of a UNS S32760 superduplex stainless steel submitted to different thermal treatments, thus leading to different percentages of the mentioned phases. A comparative study has been performed in order to evaluate the resulting mechanical properties of these phases by using hardness, microhardness and nanoindentation techniques. In addition, optical microscopy, scanning electron microscopy (SEM) and X-ray diffraction (XRD) have been also used to identify their presence and distribution. Finally, the experimental results have shown that the resulting hardness values were increased as a function of a longer heat treatment duration which it is associated to the formation of a higher percentage of the sigma phase. However, nanoindentation hardness measurements of this sigma phase showed lower values than expected, being a combination of two main factors, namely the complexity of the sigma phase structure as well as the surface finish (roughness).

Keywords: nanoindentation; hardness; duplex stainless steel; ferrite; austenite; sigma phase

1. Introduction

It is well known that an adequate percentage of austenitic (γ) and ferritic (α) phases in the resultant microstructure of duplex stainless steels play a key role in the desired final properties [1–5]. The ferrite phase provides strength and corrosion resistance, whereas the austenite phase increases the ductility. For all these reasons, duplex stainless steels are widely used in aggressive environments application such as offshore, marine, nuclear and desalination plants, among others [6–11]. However, its main drawback is the tendency to form detrimental phases at temperatures between 600 °C and 900 °C, being the cause of a significant loss of toughness and resistance to localized corrosion. One of the most known and representative detrimental phases is the precipitation of the sigma phase (σ), a Cr- and Mo-rich intermetallic compound [12–21]. This σ phase shows a tetragonal crystallographic structure with 32 atoms per unit cell [22] making possible a considerable increase in the resultant hardness,

whereas a decrease in the toughness as well as elongation is also observed [23–27]. In addition, a change in the fracture type from transgranular to intergranular is obtained as a function of higher amounts of σ phase [28].

Another important aspect is that the kinetics of sigma phase's nucleation is very fast at 850 °C due to the eutectoid decomposition of the ferrite into sigma phase and secondary austenitic phase [29–34]. As an example, A. Perron et al. [34] have studied the influence of σ phase in a 316Nb austenitic stainless steel. They observed two different mechanisms of precipitation of sigma phase. The first one involves a direct precipitation of the σ phase from the residual ferrite phase present in the material, whereas the second one is characterized by a eutectoid decomposition of the ferrite in σ phase and secondary austenite. In addition, other interesting work is presented by Nilsson et al. [2] where the kinetics of secondary phase precipitation in a super duplex stainless steel (SDSS) such as SAF 2507 is evaluated with its corresponding time-temperature-precipitation (TTP) diagram. Consequently, the micro mechanical characterization of the evolution of these phases as a specific temperature can be considered of relevant interest. On the other hand, it is necessary to point out that nanoindentation techniques are actually being developed for measuring the mechanical properties of materials on the nano-scale level [35,36] and they can be also successfully applied onto multiphase alloys for the identification of different phases as well as intermetallic compounds [37]. However, very few works can be found in the bibliography in order to have a complete and exhaustive mechanical characterization of duplex stainless steels as a function of variable thermal treatment or even in as-received condition [38–41].

Wang et al. [38] studied a duplex stainless steel in as-cast and hot-forging state with different protocol of surface preparation and chemical attacks. The results indicate that the resultant hardness in the hot-forging state was higher than in the as-cast steel, showing significant value changes in both phases. El Mehtedi [39] measured the nanohardness of a duplex stainless steel in two different conditions such as as-received and after hot deformation. They found that hardness measurement data were directly affected by the indentation size effect. Moreover, they also found a hardness ratio close to 1.2 between ferrite and austenite phases. Gadelrab [40] proposed the use of magnetic force microscopy (MFM) with the aim to clearly identify the phases based upon their different magnetic properties, before testing them by nanoindentation technique. Ferrite and austenite phases of an as-received stainless steel duplex were mechanically characterized, showing values of hardness with a low dispersion of 3.75 ± 0.23 GPa and 3.19 ± 0.16 GPa for ferrite and austenite phases, respectively. Other interesting work is presented by Guo et al. [41] where firstly it is evaluated the effect of the passive layer in ferrite and austenite phases of a 2507 duplex stainless steel. The experimental results indicated that the conductivity of the austenite phase was greater than the ferrite phase, being a less protective passive layer. Secondly, nanoindentation tests have been also performed in order to determine the mechanical properties, being the resultant hardness values of 4.41 ± 0.44 GPa and 3.57 ± 0.52 GPa for ferrite and austenite phases, respectively.

An important aspect to remark is that the nanohardness measurement of sigma phase in stainless steels has only been determined by Ohmura et al. [42,43]. In these works, it is evaluated the nano-mechanical properties of a long-term aged type 316 stainless steel. The sample was aged for 4.5 years at 700 °C, the nanohardness of the σ phase being extremely high in the order of 17 GPa. In addition, this high value of nanohardness related to σ phase can be also obtained in the grain boundary, adjoining matrix and the grain interior. Another interesting aspect is that after this long-thermal aging at 700 °C, the austenite phase has experimented a 30% hardness drop from 4.5 GPa to 3.4 GPa. However, no previous works have been found in the bibliography in order to evaluate the mechanical properties of this type of stainless steel as a function of variable time of thermal aging. This work is devoted to studying the effect of the exposition time at a fixed temperature and a further quenching step for obtaining different percentages of three specific phases such as austenite, ferrite and sigma in the duplex stainless steel. The experimental results indicate that the macrohardness as well microhardness values have been increased for longer exposition times, which is clearly associated to the formation of a higher amount of sigma phase. Finally, nanoindentation hardness measurements

of this sigma phase present lower values due to a combination of two main factors such as complexity of this structure as well as surface finish, which plays a key role in such decrease of nanohardness.

2. Experimental Section

The sample used in the present work is a UNS S32760 superduplex stainless steel tube with a dimension of 168.28 mm of external diameter and 10.97 mm of thickness. In Table 1, it can be appreciated its specific chemical composition. An important consideration is that all checked specimens used in this work are taken from in the longitudinal direction with the aim of avoiding the anisotropy's effect that could lead to erroneous interpretation of results.

Table 1. Chemical composition of the UNS S32760 superduplex stainless steel (wt % balance Fe).

Cr	Ni	Mn	Mo	Si	Cu	W	N	C	P	S
25.52	7.33	0.63	3.56	0.44	0.74	0.51	0.257	0.019	0.022	<0.003

Samples of tube cut with a dimension of 60 mm length have been used for the experimental study. Firstly, a sample in as-received state (known as S1) has been used as the reference sample; secondly, two samples have been thermally aged in a Thermolyne Type 6000 furnace (ThermoFisher Scientific, Waltham, MA, USA) at 850 °C for different periods of time of 21 min (known as S2) and 25 min (known as S3). After that, the samples were quenched in water with the aim to promote microstructures with variable percentages of σ phase. In addition, it is important to remark that the temperature at this specific value of 850 °C has been selected because it is considered the critical temperature for σ phase precipitation in superduplex stainless steels [11,16].

Samples with a specific dimension of 10.97 mm × 20 mm have been cut in axial direction, embedded in resin, polished and chemical-etched using modified Murakami reagent by immersion in a solution of 30 g KOH and 30 g of $K_3[Fe(CN)_6]$ in 60 mL of distilled water for 20 s. These samples were firstly analyzed by optical microscopy (Nikon, Midori, Japan) and the etching reveals ferrite in grey coloration, σ phase in orange-brown coloration, whereas the austenite phase is observed in white coloration. In addition, the samples were secondly characterized using a JEOL JSM-5900LV scanning electron microscopy (SEM) (JEOL, Peadoby, MA, USA) and the energy dispersive X-ray (EDX) spectroscopy (JEOL, Peadoby, MA, USA) has been used for the chemical analysis of the phases.

An X-ray diffraction (XRD) analysis has been also performed in order to corroborate the presence of the different phases of study for the different samples from S1 to S3. A Bruker D8 Discover machine (Bruker, Billerica, MA, USA) equipped with a Cr source ($\lambda_{K\alpha 1}$ = 2.2897 Å; 40 kV; 40 mA) under Bragg-Brentano configuration was used. A scan covering 2θ angles from 40° to 90° at a scan rate of 0.02° every 5 s was performed on each sample.

Conventional Vickers hardness tests for the macroscopic strength evaluation were conducted with a load of 9.8 N, while for Vickers microhardness 0.1 N was used. Five measurements were made on each phase. Nanohardness measurements were performed with a Hysitron Triboindenter TI950 (Hysitron-Bruker, Eden Prairie, MN, USA) fitted with Berkovich tip with an end radius of 150 nm. A minimum of ten indents of 5 mN of maximum load and separated enough to not influence each other were performed on each of the phases. Hardness and Young's moduli were obtained by using the method of Oliver and Pharr [35]. After the tests, the positions of the indentations were located by means of the Scanning Probe Microscopy (SPM) images that this apparatus is able to obtain using the same Berkovich pyramid as an Atomic Force Microscopy (AFM) tip.

3. Results and Discussion

3.1. Qualitative and Quantitative Analysis of the Phases

In Table 2, it can be appreciated the different percentages of all observed phases (austenite, ferrite and sigma) for the three samples of study after thermal treatment at different holding times in the

furnace at 850 °C. The sample S1 corresponds to the sample untreated thermally, in which no sigma phase is observed. The samples S2 and S3 are thermally treated with an exposition time in the furnace of 21 min and 25 min, respectively. In these thermally aged samples, higher percentages of sigma phase were observed as the exposition time is increased. It is important to remark that the kinetics of nucleation of sigma phase is very fast after 17 min of thermal treatment. There is a specific percentage change from 21 min to 25 min where sigma phase percentage significantly increases from 5.2 to 18.6 (vol %). A previous work has demonstrated how the sigma phase nucleates at the ferrite/austenite interface, growing toward the ferrite grains [19]. In addition, the experimental results also reveal that the ferrite phase percentage decreases in an opposite tendency to sigma phase and in a similar magnitude. This phenomenon is associated to the decomposition that ferrite experiments to form sigma phase and secondary austenite [16,44,45]. The objective of different percentages of sigma phase precipitated is to analyze the behavior of the phases in the first stages of sigma phase nucleation in α-α as well as α-ɣ boundaries, and in the subsequent stage, where the sigma phase grows towards the ferrite phase. Finally, the purpose of these thermal treatments with a short variation in time was to provide samples corresponding to these two different stages.

Table 2. Percentage of austenite, ferrite and sigma phases (vol %) as received (S1) and after thermal treatment at a different interval of time (S2 and S3, respectively).

Sample Identification	Time (min)	Austenite	Ferrite	Sigma
S1	0	43.0 ± 1.8	57.0 ± 1.8	0 ± 0.0
S2	21	44.9 ± 2.9	49.9 ± 3.2	5.2 ± 0.8
S3	25	41.2 ± 3.9	40.2 ± 2.9	18.6 ± 1.8

In order to corroborate the presence of sigma phase in the samples as a function of the thermal treatment, a XRD analysis has been performed for all the samples of study. In Figure 1, a zoom of the main region of interest, where the presence of peaks that can be linked to the sigma phase for the samples S2 and S3 appear, is shown. On the contrary, S1 with no content of sigma phase does not show such peaks and only shows the typical fingerprint for alpha and gamma phases. In this Figure, it can be clearly observed that S2 (5.2 vol % σ phase) and S3 (18.6 vol % σ phase) show the peaks for such phase together with the ones for the alpha and gamma phases, typical of these types of stainless steels. On the contrary, S1 with 0% of sigma phase does not show the sigma peaks. Finally, some small peaks marked with R can be attributed to the resin where the samples are hot mounted prior to the analysis. The only sample not showing these peaks is S3, because it has not been hot mounted for the XRD analysis.

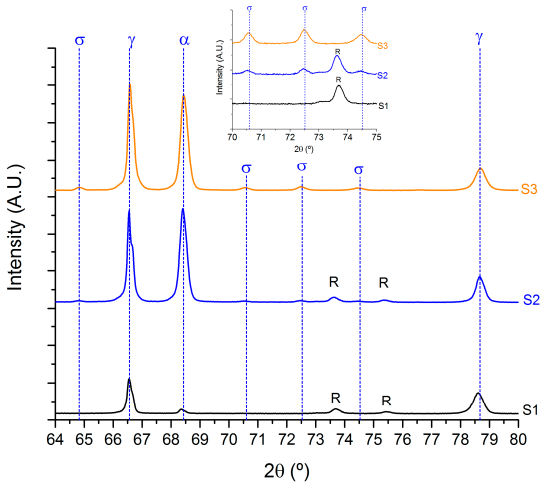

Figure 1. X-ray diffraction patterns for samples from S1 to S3 using a Cr source ($\lambda_{K\alpha 1}$ = 2.2897 Å). The "R" symbols refer to some peaks coming from the resin where samples S1 and S2 are hot mounted.

In addition, SEM analysis has also been carried out for the identification of the most representative phases in the stainless steel. Figure 2 shows the SEM images for all the samples of study (S1, S2 and S3, respectively). The micrographs obtained from SEM images by using backscattered electrons indicate the presence of three different secondary phases precipitated in the microstructure. The first one corresponds to the chi phase (χ) with a white coloration. The second one corresponds to sigma phase, showing a gray coloration, and the third one corresponds to chromium nitride (Cr_2N) which appears with a black coloration. In addition, it can also be observed that both chi phase and nitrides grow along the austenite/ferrite boundary, whereas the sigma phase nucleates preferentially at the ferrite/austenite interfaces and then grows through the ferrite phase [19]. Finally, the identification of the phases shown in Figure 2 has been confirmed by an EDX analysis. In Table 3, the chemical composition distribution of the sigma phase after all thermal treatments point out is shown. A main conclusion obtained by the chemical analysis is that the percentage of chromium and molybdenum are gradually increased in the sigma phase when the time of thermal treatment is increased from 21 min to 25 min, respectively.

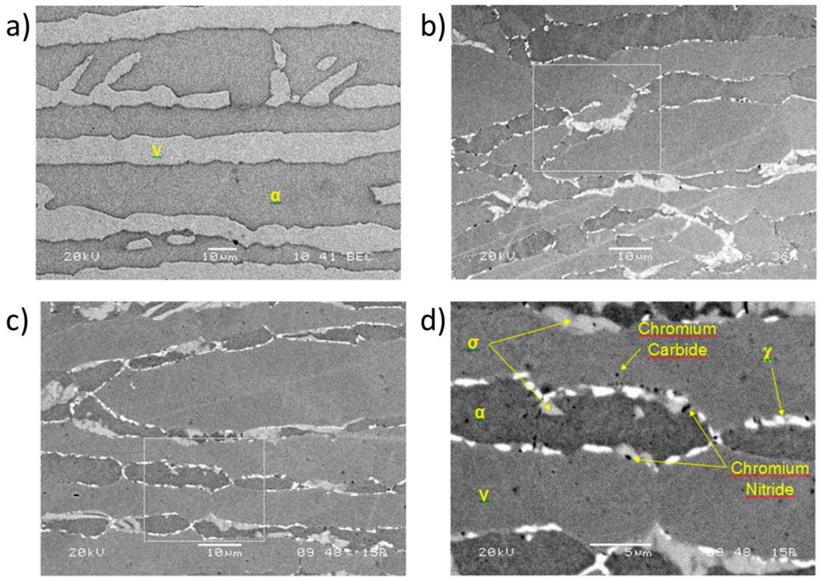

Figure 2. SEM images using backscattered electrons for the untreated sample (as received, S1) (**a**); sample aged for a period of time of 21 min (S2) (**b**); sample aged for a period of time of 25 min (S3) (**c**); and a zoom of the region of interest of S3 for a better appreciation of the secondary phases in the austenite/ferrite matrix (**d**). The white rectangles mark the zone where the zoom is performed.

Table 3. EDX analysis showing the evolution of the chemical composition of the sigma phase as a function of the time thermal treatment from 21 min to 25 min (wt %).

Thermal Treatment at 850 °C (min)	Phase	Si	Cr	Fe	Ni	Mo	W
S2 (21 min)	σ	0.46	28.72	59.44	5.64	4.85	0.88
S3 (25 min)	σ	0.36	30.73	56.52	4.72	6.59	0.56

Once it has corroborated the presence of the sigma phase for XRD as well as SEM analysis for being the phase of interest in this study, the next step is to determine the mechanical properties for this σ phase by using different techniques such as macrohardness, microhardness and nanoindentation tests.

3.2. Hardness Measurements

In Figure 3, it is shown the results of hardness Vickers for all the samples of study from S1 to S3 with their corresponding standard deviation. For the first thermal treatment of 21 min (S1), the

duplex stainless steel presents a notable increase of hardness value from 248 ± 2.34 to 269 ± 4.34 in comparison with the untreated sample S1. However, this increase is more severe for the sample aged for a longer period of time (S3) where the hardness value presents the highest value of 298 ± 3.93, which corresponds to an overall increase of 20.16% in comparison with the sample without thermal aging.

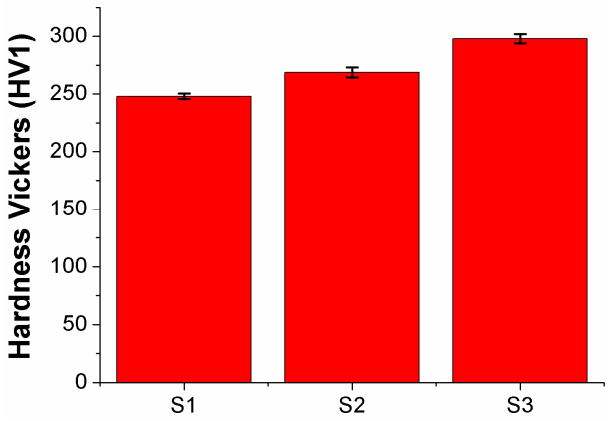

Figure 3. Macrohardness Vickers values for all the samples of study (S1, S2 and S3).

3.3. Microhardness Measurements

In Figure 4, it can be observed the micro-indentations Vickers in austenite, ferrite and sigma phases, respectively. An important aspect to remark is that the microhardness of sigma phase has only been measured in the samples S2 and S3 for showing a representative percentage of this specific phase.

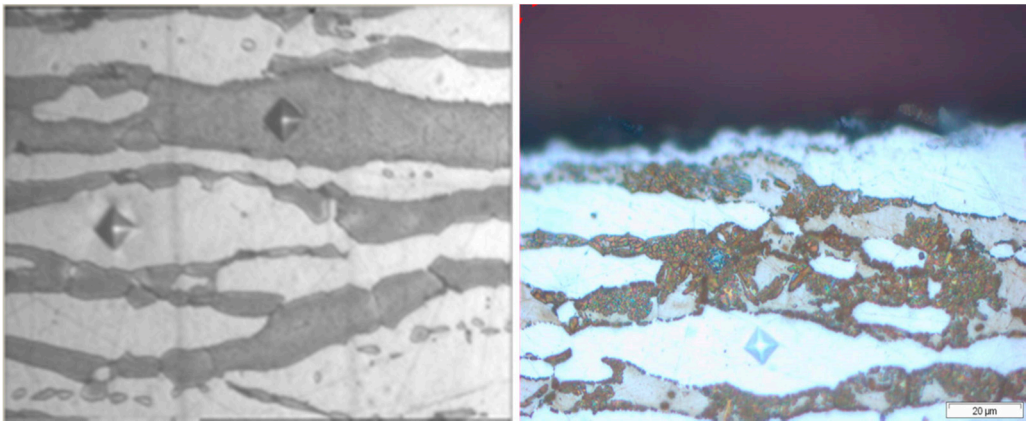

(**a**) (**b**)

Figure 4. Optical micrograph of the Vickers micro-indentations in austenite phase (white) and ferrite phase (grey) for sample S1 (**a**); Optical micrograph of the Vickers micro-indentations in austenite phase (white) and sigma phase (brown) for the sample S3 (**b**).

In Figure 5, it can be observed the microhardness Vickers values for all the samples of study (S1, S2 and S3). The experimental results clearly indicate that no significant differences in the hardness values are observed for the austenite and ferrite phases for all the samples. In addition, higher values of microhardness are observed for ferrite phase in comparison with the austenite phase. Another interesting result is that the sigma phase shows a considerable increase in microhardness from 315.3 HV for S2 to 427.4 HV for S3. A main conclusion that can be obtained from these experimental data is that a longer time of thermal aging makes possible a higher amount of sigma phase and, as a result (see Table 2), an increase of the resultant microhardness values are obtained. However, this

experimental result related to this sigma phase is lower than reported by Guimaraes et al. [46], who measured values of 522 HV in an AISI 446 stainless steel.

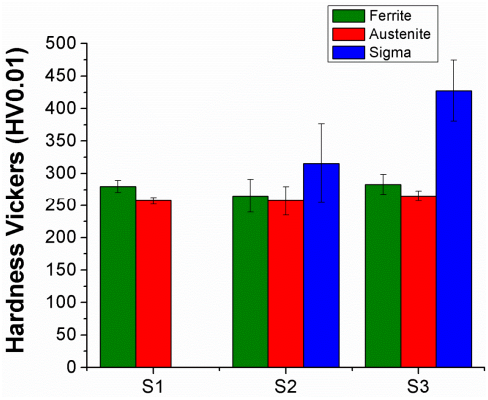

Figure 5. Microhardness Vickers values in ferrite, austenite and sigma phases for all samples of study.

3.4. Nanoindentation Measurements

3.4.1. Nanoindentation Hardness Measurements in Austenite and Ferrite Phases

SPM images, managed with WSxM (Nanotech) program, of austenite as well as ferrite phases of all the samples of study are shown in Figure 6.

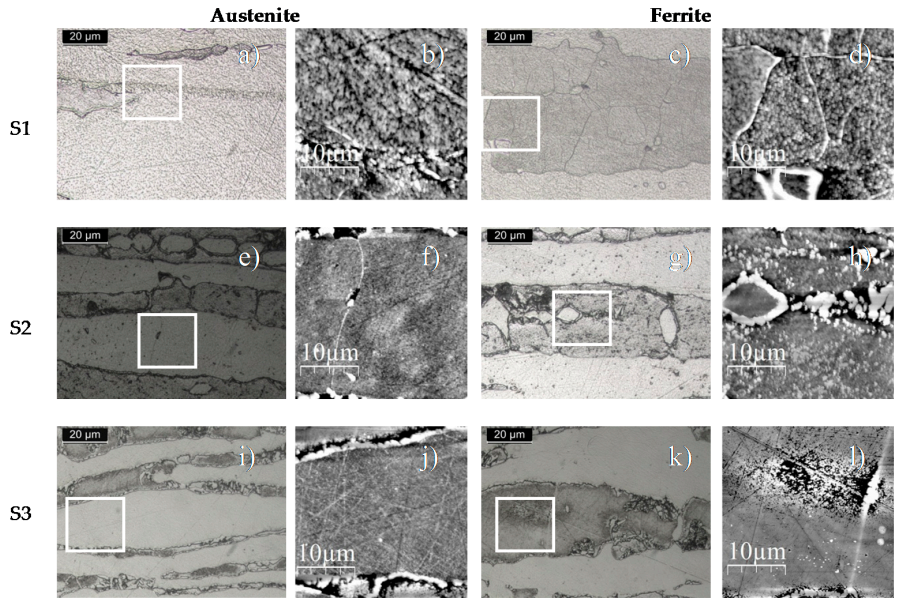

Figure 6. Selected zones of austenite and ferrite phases for nanohardness measurements: S1 (**a**–**d**); S2 (**e**–**h**) and S3 (**i**–**l**), respectively. White rectangles in the optical images (left ones) mark the zone where AFM images have been obtained (right ones).

It is possible to observe the evolution of the experimental results related to the nanohardness of the ferrite phase as well as austenite phase in Figure 7. First of all, it can be observed that the initial values of nanohardness related to both phases in S1 are very similar with an average of 6.2 GPa. These specific values of nanohardness are higher than other values presented in previous works from 3.2 GPa to 4.4 GPa [26,27]. The main reason to justify this observation is based on work-hardening applied onto the stainless steel pipe during its manufacturing process. The evolution

of the nanohardness is progressively increased from 6.25 ± 0.25 GPa (S2) to 6.75 ± 0.35 GPa (S3) for austenite phase and from 6.46 ± 0.08 GPa (S2) to 6.98 ± 0.43 GPa (S3) for ferrite phase. These values with this gradual increase of nanohardness for all the samples are coherent with the values obtained by microhardness measurements.

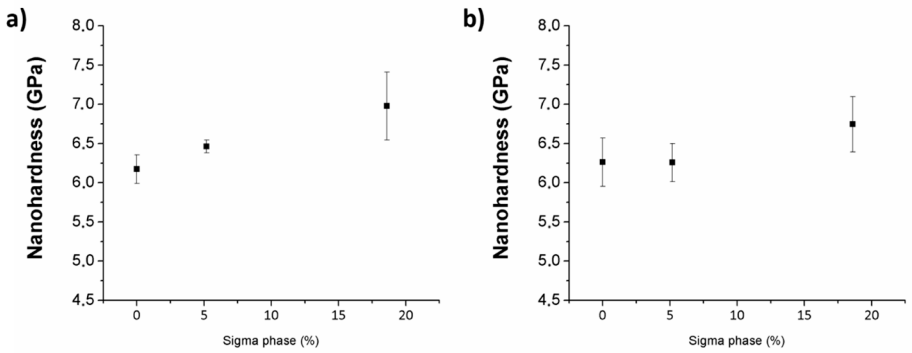

Figure 7. Average nanohardness evolution of ferrite (**a**) and austenite (**b**) vs. sigma phase percentage.

3.4.2. Nanoidentation Hardness Measurements in Sigma Phase

In Figure 8, it is shown a micrograph of the surface of S3 where some sigma phase grains are clearly visible, growing within the ferrite grains. In addition, Figure 8b presents an AFM height signal image of the same grain where the morphology of the phase is clearly visible. Finally, Figure 8c is the corresponding image picturing the phase signal. All 1 mN indentations for sigma phase have been performed on the dark grey surfaces such as the ones that can be appreciated in this image. The experimental results of the average nanoindentation hardness value obtained for a maximum load of 1 mN for the sigma grains is 7.3 ± 1.5 GPa, if we consider both S2 and S3. A combination of two main reasons might explain the low nanoindentation hardness and the high relative standard deviation of the results. Firstly, it has been previously reported [46] that the sigma phase may present a wide range of hardness values due to the complexity of this structure. Secondly, nanoindentation results are strongly dependent on the surface finish, especially affecting the scattering of the results with respect to the average value [47] but not only, since both the hardness and Young's modulus are strongly influenced. Moreover, the average is considered low as it is expectable that the hardness of an intermetallic compound as sigma phase is higher. Only two of the measurements—out of twenty—with a value close to 10.8 GPa, can be considered close to the hardness value of an intermetallic compound.

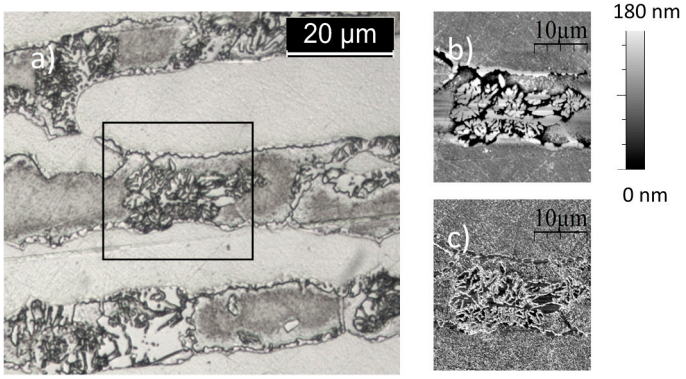

Figure 8. (**a**) Optical image of sigma phase for S3 (black rectangle). (**b**) Atomic Force Microscopy (AFM) image—height signal—of the previous sigma grain (**c**) AFM image (phase signal) of the previous sigma grain. Indents have been performed on the dark grey grains of this last image. White rectangles in the optical images (left ones) mark the zone where AFM images have been obtained (right ones).

4. Conclusions

In this work, the hardness, microhardness and nanohardness values of three samples (known as S1, S2 and S3) related to UNS 32706 duplex stainless steels is evaluated. These samples have been exposed to different periods of time at a fixed temperature of 850 °C and then, all of them have been performed to a further water quenching step. As a result, variable percentages of three specific phases such as austenite, ferrite and sigma are varied as a function of the exposition time from 0, 21 and 25 min. The experimental results indicate that longer exposition times make possible the precipitation of a higher percentage of sigma phase, which plays a key role in the resultant values of hardness. Firstly, it has been observed a high macrohardness value for the samples with a longer thermal aging, which is associated to the increase of hardness related to ferrite and austenite phases as well as nucleation and propagation of sigma phase. Secondly, microhardness values also corroborate the results obtained by macrohardness values because higher values of microhardness have been obtained, especially for sigma phase, where an important increase from 315 HV to 427 HV has been obtained as a function of the presence of a higher amount of sigma phase in the resultant microstructure. Finally, the measurements of nanohardness of sigma phase show lower values than expected due to the high roughness of this phase. It is proposed to make a more aggressive protocol to provide specific properties of surface and reduce this surface effect, making it possible to acquire hardness measurements of this phase correctly.

Author Contributions: Gorka Argandoña carried out the main part of the experimental work, including SEM, EDX and hardness measurements. Gorka Argandoña participated in the design of the study and in the draft of the manuscript. José F. Palacio carried the main part of the experimental work, including the XRD analysis, microhardness and nanohardness measurements. Julio Peña participated in the experimental work. Carlos Berlanga, María V. Biezma, Pedro J. Rivero and Rafael Rodriguez participated in the design of the study and helped with the draft of the manuscript.

Conflicts of Interest: The authors declare no conflict of interest.

References

1. Nilsson, J.-O. Super Duplex Stainless Steels. *Mater. Sci. Technol.* **1992**, *8*, 685–700. [CrossRef]
2. Nilsson, J.O.; Wilson, A. Influence of isothermal phase transformations on toughness and pitting corrosion of super duplex stainless steel SAF 2507. *Mater. Sci. Technol.* **1993**, *9*, 545–554. [CrossRef]
3. Han, Y.; Zou, D.; Yao, H.; Zhang, W.; Yu, J. Microstructural evolutions and its influence on properties of super-duplex stainless steel. *Adv. Mater. Res.* **2010**, *97*, 656–659. [CrossRef]
4. Li, X.; Miodownik, A.P.; Saunders, N. Modelling of materials properties in duplex stainless steels. *Mater. Sci. Technol.* **2002**, *18*, 861–868.
5. Silva, E.M.; Marinho, L.B.; Rebouças Filho, P.P.; Leite, J.P.; Leite, J.P.; Fialho, W.M.L.; de Albuquerque, V.H.C.; Tavares, J.M.R.S. Classification of induced magnetic field signals for the microstructural characterization of sigma phase in duplex stainless steels. *Metals* **2016**, *6*, 164. [CrossRef]
6. Olabi, A.G.; Lostado, R.; Benyounis, K.Y. Review of microstructures, mechanical properties, and residual stresses of ferritic and martensitic stainless-steel welded joints. *Compr. Mater. Process.* **2014**, *6*, 181–192.
7. Alvarez, S.M.; Bautista, A.; Velasco, F. Corrosion behaviour of corrugated lean duplex stainless steels in simulated concrete pore solutions. *Corros. Sci.* **2011**, *53*, 1748–1755. [CrossRef]
8. Olsson, J.; Snis, M. Duplex—A new generation of stainless steels for desalination plants. *Desalination* **2007**, *205*, 104–113. [CrossRef]
9. Dabalà, M.; Calliari, I.; Variola, A. Corrosion behavior of a superduplex stainless steel in chloride aqueous solution. *J. Mater. Eng. Perform.* **2004**, *13*, 237–240. [CrossRef]
10. Machuca, L.L.; Bailey, S.I.; Gubner, R.; Watkin, E.L.J.; Ginige, M.P.; Kaksonen, A.H. Crevice corrosion of duplex stainless steels in the presence of natural marine biofilms. *NACE Int. Corros. Conf. Ser.* **2012**, *5*, 3924–3936.
11. Veljkovic, M.; Gozzi, J. Use of duplex stainless steel in economic design of a pressure vessel. *J. Press. Vessel Technol.* **2007**, *129*, 155–161. [CrossRef]
12. Saithala, J.R.; Mahajanam, S.; Ubhi, H.S.; Atkinson, J. Environmental assisted cracking behavior of sigmatized super duplex stainless steel in oilfield production brine. *Corrosion* **2013**, *69*, 276–285. [CrossRef]

13. Yang, S.-M.; Chen, Y.-C.; Chen, C.-H.; Huang, W.-P.; Lin, D.-Y. Microstructural characterization of $\delta/\gamma/\sigma/\gamma 2/\chi$ phases in silver-doped 2205 duplex stainless steel under 800 °C aging. *J. Alloys Compd.* **2015**, *633*, 48–53. [CrossRef]
14. Jeon, S.-H.; Kim, S.-T.; Lee, I.-S.; Kim, J.-S.; Kim, K.-T.; Park, Y.-S. Effects of Cu on the precipitation of intermetallic compounds and the intergranular corrosion of hyper duplex stainless steels. *Corros. Sci.* **2013**, *66*, 217–224. [CrossRef]
15. Kim, S.-K.; Kang, K.-Y.; Kim, M.-S.; Lee, J.-M. Low-temperature mechanical behavior of super duplex stainless steel with sigma precipitation. *Metals* **2015**, *5*, 1732–1745. [CrossRef]
16. Michalska, J.; Sozańska, M. Qualitative and Quantitative Analysis of σ and χ Phases in 2205 Duplex Stainless Steel. *Mater. Charact.* **2006**, *56*, 355–362. [CrossRef]
17. Ferro, P.; Bonollo, F.; Timelli, G. Sigma phase precipitation modelling in a UNS S32760 superduplex stainless steel. *Metall. Ital.* **2012**, *104*, 7–12.
18. Elsabbagh, F.M.; Hamouda, R.M.; Taha, M.A. On microstructure and microhardness of isothermally aged UNS S32760 and the effect on toughness and corrosion behavior. *J. Mater. Eng. Perform.* **2014**, *23*, 275–284. [CrossRef]
19. Argandona, G.; Biezma, M.V.; Berrueta, J.M.; Berlanga, C.; Ruiz, A. Detection of secondary phases in UNS S32760 superduplex stainless steel by destructive and non-destructive techniques. *J. Mater. Eng. Perform.* **2016**, *25*, 5269–5279. [CrossRef]
20. Llorca-Isern, N.; López-Jiménez, I.; López-Luque, H.; Biezma, M.V.; Roca, A. Study of the precipitation of secondary phases in duplex and superduplex stainless steel. *Mater. Sci. Forum* **2017**, *879*, 2537–2542. [CrossRef]
21. Llorca-Isern, N.; López-Luque, H.; López-Jiménez, I.; Biezma, M.V. Identification of sigma and chi phases in duplex stainless steels. *Mater. Charact.* **2016**, *112*, 20–29. [CrossRef]
22. Atamert, S.; King, J.E. Sigma-phase formation and its prevention in duplex stainless steels. *J. Mater. Sci. Lett.* **1993**, *12*, 1144–1147. [CrossRef]
23. Lee, J.; Kim, I.; Kimura, A. Application of small punch test to evaluate sigma-phase embrittlement of pressure vessel cladding material. *J. Nucl. Sci. Technol.* **2003**, *40*, 664–671. [CrossRef]
24. Liu, T.; Zhiyong, R.W.; Xu, D.; Aung, A.A. Metallurgical analysis on a cracked super duplex stainless steel flange. *J. Fail. Anal. Prev.* **2014**, *14*, 470–477. [CrossRef]
25. Pohl, M.; Storz, O.; Glogowski, T. Effect of Intermetallic Precipitations on the Properties of Duplex Stainless Steel. *Mater. Charact.* **2007**, *58*, 65–71. [CrossRef]
26. Maehara, Y.; Koike, M.; Fujino, N.; Kunitake, T. Precipitation of sigma phase in a 25Cr-7Ni-3Mo duplex phase stainless steel. *Trans. Iron Steel Inst. Jpn.* **1983**, *23*, 240–246. [CrossRef]
27. Wilms, M.E.; Gadgil, V.J.; Krougman, J.M.; Kolster, B.H. The effect of σ-phase precipitation at 800 °C on the mechanical properties of a high alloyed duplex stainless steel. *Mater. High Temp.* **1991**, *9*, 160–166. [CrossRef]
28. Biezma, M.V.; Berlanga, C.; Argandona, G. Relationship between microstructure and fracture types in a UNS S32205 duplex stainless steel. *Mater. Res.* **2013**, *16*, 965–969. [CrossRef]
29. Berecz, T.; Mészáros, I.; Szabó, P.J. Decomposition of the ferritic phase in isothermally aged SAF 2507 duplex stainless steel. *Mater. Sci. Forum* **2008**, *589*, 185–190. [CrossRef]
30. Berecz, T.; Fazakas, É.; Mészáros, I.; Sajó, I. Decomposition kinetics of ferrite in isothermally aged SAF 2507-type duplex stainless steel. *J. Mater. Eng. Perform.* **2015**, *24*, 4777–4788. [CrossRef]
31. Chandra, K.; Kain, V.; Bhutani, V.; Raja, V.S.; Tewari, R.; Dey, G.K.; Chakravartty, J.K. Low temperature thermal aging of austenitic stainless steel welds: Kinetics and effects on mechanical properties. *Mater. Sci. Eng. A* **2012**, *534*, 163–175. [CrossRef]
32. Morris, D. The influence of sigma phase on creep ductility in type 316 stainless steel. *Scr. Metall.* **1979**, *13*, 1195–1196. [CrossRef]
33. May, V.E. Sigma phase embrittlement of austenitic stainless steel FCCU regenerator internals. *Mater. Perform.* **1985**, *24*, 18–22.
34. Perron, A.; Toffolon-Masclet, C.; Ledoux, X.; Buy, F.; Guilbert, T.; Urvoy, S.; Bosonnet, S.; Marini, B.; Cortial, F.; Texier, G.; et al. Understanding sigma-phase precipitation in a stabilized austenitic stainless steel (316Nb) through complementary CALPHAD-based and experimental investigations. *Acta Mater.* **2014**, *79*, 16–29. [CrossRef]

35. Oliver, W.C.; Pharr, G.M. Measurement of hardness and elastic modulus by instrumented indentation: Advances in understanding and refinements to methodology. *J. Mater. Res.* **2004**, *19*, 3–20. [CrossRef]
36. Oliver, W.C.; Pharr, G.M. Nanoindentation in materials research: Past, present, and future. *MRS Bull.* **2010**, *35*, 897–907. [CrossRef]
37. Furnémont, Q.; Kempf, M.; Jacques, P.J.; Göken, M.; Delannay, F. On the measurement of the nanohardness of the constitutive phases of trip-assisted multiphase steels. *Mater. Sci. Eng. A* **2002**, *328*, 26–32. [CrossRef]
38. Wang, X.F.; Yang, X.P.; Guo, Z.D.; Zhou, Y.C.; Song, H.W. Nanoindentation characterization of mechanical properties of ferrite and austenite in duplex stainless steel. *Adv. Mater. Process.* **2007**, *26*, 1165–1171. [CrossRef]
39. El Mehtedi, M.; Spigarelli, S.; Ricci, P.; Paternoster, C.; Quadrini, E. Mechanical characterization of phases in duplex 2205 stainless steel by nanoindentation technique. *Metall. Ital.* **2010**, *102*, 11–16.
40. Gadelrab, K.R.; Li, G.; Chiesa, M.; Souier, T. Local characterization of austenite and ferrite phases in duplex stainless steel using MFM and nanoindentation. *J. Mater. Res.* **2012**, *27*, 1573–1579. [CrossRef]
41. Guo, L.Q.; Lin, M.C.; Qiao, L.J.; Volinsky, A.A. Ferrite and austenite phase identification in duplex stainless steel using SPM techniques. *Appl. Surf. Sci.* **2013**, *287*, 499–501. [CrossRef]
42. Ohmura, T.; Tsuzaki, K.; Sawada, K.; Kimura, K. Inhomogeneous nano-mechanical properties in the multi-phase microstructure of long-term aged type 316 stainless steel. *J. Mater. Res.* **2006**, *21*, 1229–1236. [CrossRef]
43. Ohmura, T.; Sawada, K.; Kimura, K.; Tsuzaki, K. Alteration in nanohardness of matrix phase associated with precipitation during long-term aging of type 316 stainless steel. *Mater. Sci. Eng. A* **2008**, *489*, 85–92. [CrossRef]
44. Peguet, L.; Gaugain, A. Localized corrosion resistance of duplex stainless steels: Methodology and properties; a review paper. *Rev. Metall.* **2011**, *108*, 231–243. [CrossRef]
45. Fang, Y.L.; Liu, Z.Y.; Xue, W.Y.; Song, H.M.; Jiang, L.Z. Precipitation of secondary phases in lean duplex stainless steel 2101 during isothermal ageing. *ISIJ Int.* **2010**, *50*, 286–293. [CrossRef]
46. Guimarães, A.A.; Mei, P.R. Precipitation of carbides and sigma phase in AISI type 446 stainless steel under working conditions. *J. Mater. Process. Technol.* **2004**, *155*, 1681–1689. [CrossRef]
47. Walter, C.; Mitterer, C. 3D versus 2D finite element simulation of the effect of surface roughness on nanoindentation of hard coatings. *Surf. Coat. Technol.* **2009**, *203*, 3286–3290. [CrossRef]